The Moist Available Energy of a Conditionally Unstable Atmosphere. Part II: Further Analysis of GATE Data

JUNYI WANG AND DAVID A. RANDALL

Department of Atmospheric Science, Colorado State University, Fort Collins, Colorado

(Manuscript received 5 April 1993, in final form 9 August 1993)

ABSTRACT

The generalized convective available potential energy (GCAPE) observed during GATE has been analyzed using the Lagrangian algorithm of Lorenz, as modified by Randall and Wang. The effects of ice are included and are discussed in an Appendix. A high positive correlation is found between the rate of GCAPE production by large-scale processes and the observed precipitation rate, and a negative correlation between the GCAPE itself and the precipitation rate. The observed time rate of change of the GCAPE is much smaller than the rate of GCAPE production by large-scale processes.

1. Introduction

Lorenz (1955) defined the available potential energy (APE) as the difference between the actual total enthalpy of the atmosphere and the minimum total enthalpy that could be achieved by rearranging the mass under reversible adiabatic processes. The state of minimized enthalpy, which he called the "reference state," is also the state of maximized kinetic energy. The APE represents the portion of the nonkinetic energy that is available for conversion into kinetic energy under reversible adiabatic processes.

Recognizing that moist-adiabatic processes are, in fact, adiabatic rather than diabatic, Lorenz (1978, 1979) extended the concept of APE to the moist atmosphere, coining the term "moist available energy" (MAE). The MAE depends on both the horizontal and vertical structures of the atmosphere. As discussed by Randall and Wang (1992; hereafter referred to as Part I), the vertical "component" of the MAE (i.e., the MAE that can be detected by considering only the vertical structure of an atmospheric column) is a generalization of the convective available potential energy (CAPE), which we refer to as the generalized CAPE or GCAPE. It represents the potential energy available for convection. Unlike conventional measures of CAPE, the GCAPE includes the effects of multiple parcels originating at multiple levels, and also the effects of compensating motions in the environment. We have modified the algorithm to include the effects of ice, following the method of Ooyama (1990); see the Appendix for an explanation.

Corresponding author address: Dr. David A. Randall, Department of Atmospheric Science, Colorado State University, Fort Collins, CO 80523.

In this paper, we report a further study of the variations of the GCAPE in the GATE data. The data used are from GATE Phase III, for each of 157 observation times, which span every three hours from 0900 UTC 30 August to 2100 UTC 18 September 1974 (Thompson et al. 1979).

2. Method

As demonstrated in Part I, the GCAPE can be calculated by using the parcel-moving algorithm designed by Lorenz (1979). Hereafter we refer to this as the "L" algorithm, where the "L" can be interpreted as standing for either Lorenz or Lagrangian. The details of the L algorithm are described in Part I; a brief summary is as follows. A given sounding is divided into many layers, which are adiabatically and reversibly rearranged in a Lagrangian sense, that is, moved to different pressures, in such a way as to minimize the total enthalpy; see Fig. 1. Because the layers are treated as discrete units that maintain their identities in passing from the given state to the reference state, we can refer to them as "parcels." The method used to find the vertical ordering of the parcels in the reference state is a slightly modified version of the method suggested by Lorenz (1979); see Part I for an explanation. The GCAPE is determined as the difference in total enthalpy between the given state and the reference state. The L algorithm guarantees that the reference state is horizontally homogeneous, although it may have very fine vertical structure.

The L algorithm is approximate in that the continuous atmosphere is represented by a finite number of parcels; except for this discretization, the algorithm is essentially exact. Results presented in Part I, and further results to be presented in this paper, show that the

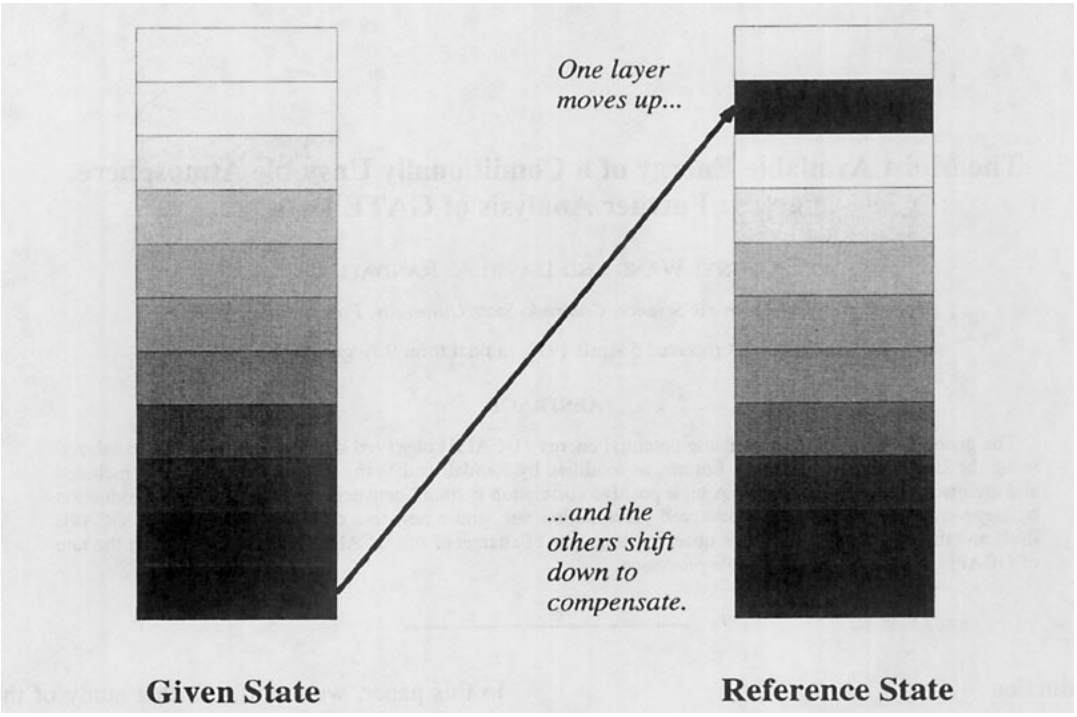

FIG. 1. Diagram illustrating the L algorithm. Layers or "parcels" of the given state are bodily reordered in the reference state.

GCAPE and reference sounding converge, that is, become independent of the number of parcels, as the number of parcels increases.

3. Results

First we present some results obtained with a particular GATE Phase III sounding, that for observation time 45, which is 2100 UTC 4 September 1974. This sounding was chosen because the GCAPE is particularly large (see results presented later).

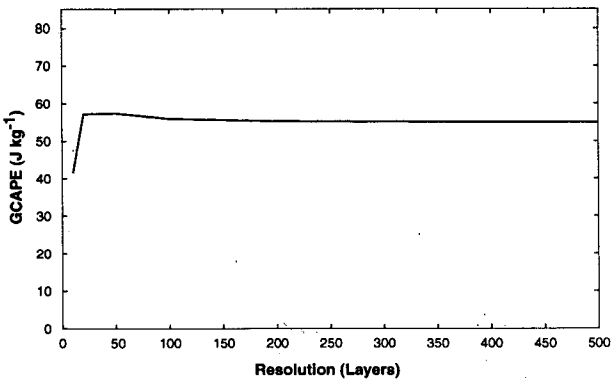

FIG. 2. The resolution dependence of the GCAPE, for GATE observation time 45. Results are plotted for up to 500 layers. The smallest number of layers considered is ten.

Figure 2 shows the resolution dependence of the GCAPE obtained with the L algorithm. Results are plotted for up to 500 layers; the smallest number of layers considered here is ten. Convergence is good with 40 layers, and excellent with 100 or more layers. The GCAPE detected is about 55 J kg^{-1}.

The dependence of the GCAPE on the vertical distributions of temperature and total mixing ratio in the given state is obviously of interest. Figure 3 shows the change of GCAPE obtained by altering the temperature or total mixing ratio, as a function of the height at which the change is made, again for GATE observation time 45. As expected, increasing the low-level temperature (or entropy) increases the GCAPE, as does decreasing the upper-level temperature (or entropy). Increasing the low-level moisture also increases the GCAPE. Increasing the moisture aloft has little effect, however.

Now we analyze the Phase III data for each observation time (every 3 hours) from 0 UTC 1 September (observation time 14) to 2100 UTC 18 September 1974 (observation time 157). We use 40 layers.

Figure 4 shows the time variation of the GCAPE. Also shown, for comparison, is the radar-observed precipitation rate. Temporal fluctuations over GATE Phase III span roughly one order of magnitude. The correlation of the GCAPE with the observed precipitation rate is −0.43. A similar result was reported by Thompson et al. (1979). The implication is that the level of convective activity, as measured by the precip-

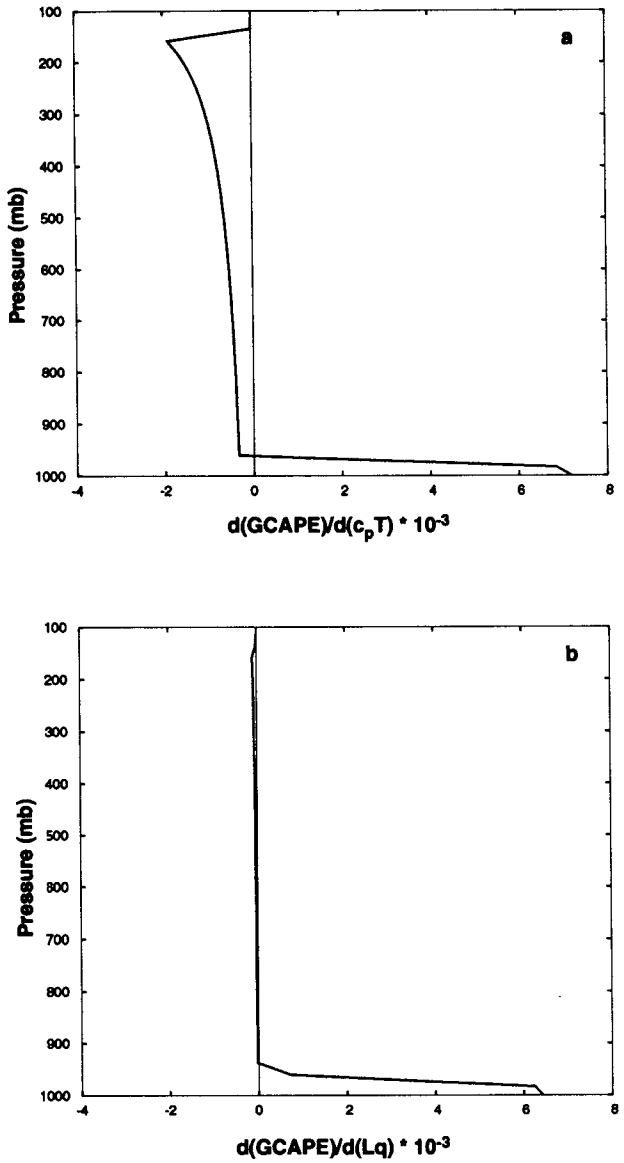

FIG. 3. The rate of change of the GCAPE with the temperature (panel a) and total mixing ratio (panel b), plotted as a function of the pressure at which the change is made, for GATE Phase III observation time 45.

itation rate, does not simply increase with the degree of convective instability; if anything, it decreases. An interpretation is that the observed degree of convective instability is strongly influenced by the rate at which convection consumes GCAPE.

We have investigated the effects of "large-scale" (i.e., nonconvective) processes on the GCAPE by the following method. First, we determine the GCAPE associated with an observed sounding. Then we consider the effects of the various nonconvective processes such as advection of temperature and moisture, adiabatic expansion, surface fluxes, and radiation. The large-scale tendencies were obtained from the GATE analyses of Thompson et al. (1979). Radiative effects were based on the GATE radiative heating (cooling) rates calculated by Cox and Griffith (1979a,b). The surface evaporation rate and the surface sensible heat flux were obtained from Dr. E. E. Recker of the University of Washington (1992, personal communication), based on analysis of ship data by Thompson (1977). These surface fluxes were assumed to act uniformly on the air between the surface and 950 mb. For each observation time, we determined the GCAPE of a hypothetical sounding, defined as the given sounding as modified by the effects of the *nonconvective processes only,* acting over a time interval Δt. The difference of the GCAPEs between the hypothetical sounding and the observed sounding, divided by Δt, is considered to be the rate of GCAPE production by large-scale processes. We choose $\Delta t = 3$ h, simply because the observations are available every three hours. The effects of the choice of Δt are discussed at the end of this section.

Figure 5a shows the time variation of the GCAPE production rate due to all nonconvective processes. Also shown, for comparison, is the radar-observed precipitation rate. There is a strong positive correlation between the rate of GCAPE production by large-scale processes and the observed precipitation rate. The correlation coefficient is 0.79. Figure 5b shows the GCAPE production rate with and without the effects of surface evaporation. The overall GCAPE production rate is greatly enhanced by the effects of surface evaporation, although its temporal fluctuations are mainly controlled by other processes.

For GATE observation time 45, Fig. 6 shows the contributions of various processes to the GCAPE production rate. The effects of large-scale vertical motion on temperature and moisture are powerful GCAPE producers, increasing the given value (55.79 J kg^{-1}) by about two-thirds (to 88.94 J kg^{-1}) in three hours. Surface evaporation is of even greater importance. Radiation and the surface sensible heat flux are very minor contributors; this is consistent with the conclusions of

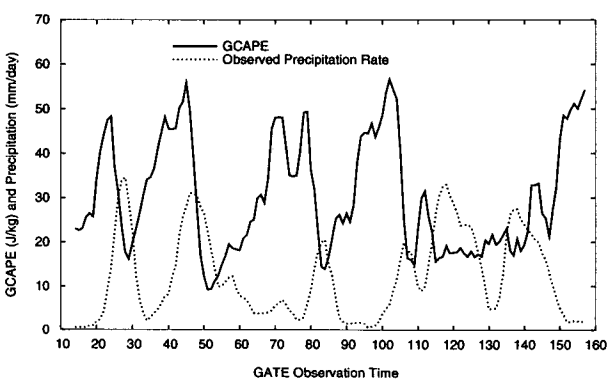

FIG. 4. The time variation of the GCAPE during GATE Phase III. Also shown, for comparison, is the radar-observed precipitation rate.

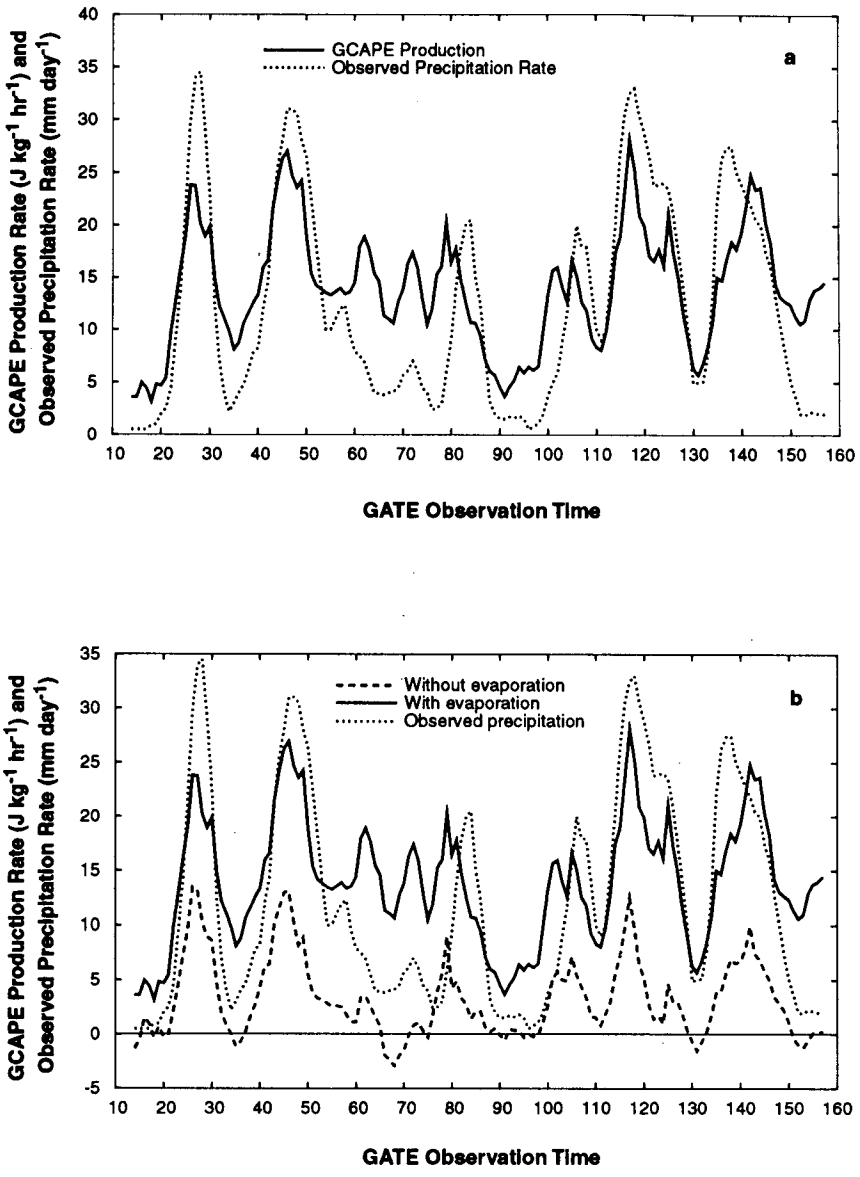

FIG. 5. (a) The time variation of the GCAPE production rate due to large-scale processes, including advection, radiation and surface fluxes, as determined. Also shown, for comparison, is the radar-observed precipitation rate. (b) The time variation of the GCAPE production rate with and without the effects of surface evaporation. The zero line is shown, for convenience. Also plotted, for comparison, is the radar-observed precipitation rate.

Lord (1982). Of course, the contributions of the various processes, as shown in Fig. 6, depend to some extent on the order in which the processes are included, but the basic conclusions given above are not sensitive to the order.

Figure 7 shows a comparison of the rate of GCAPE production by large-scale processes and the observed rate of change of the GCAPE. Each point in the figure represents one observation time. The value on the ordinate represents the observed time rate of change of the GCAPE, while the value on abscissa represents the rate of GCAPE production by large-scale processes. It is apparent that the rate of GCAPE production by large-scale processes is generally much greater than the observed time rate of change of the GCAPE. A similar conclusion was reached by Arakawa and Schubert (1974), Lord (1982), and Xu and Arakawa (1992). The results shown in Fig. 7 imply that there is a very strong negative correlation between the time rate of change of the GCAPE due to convection and that due

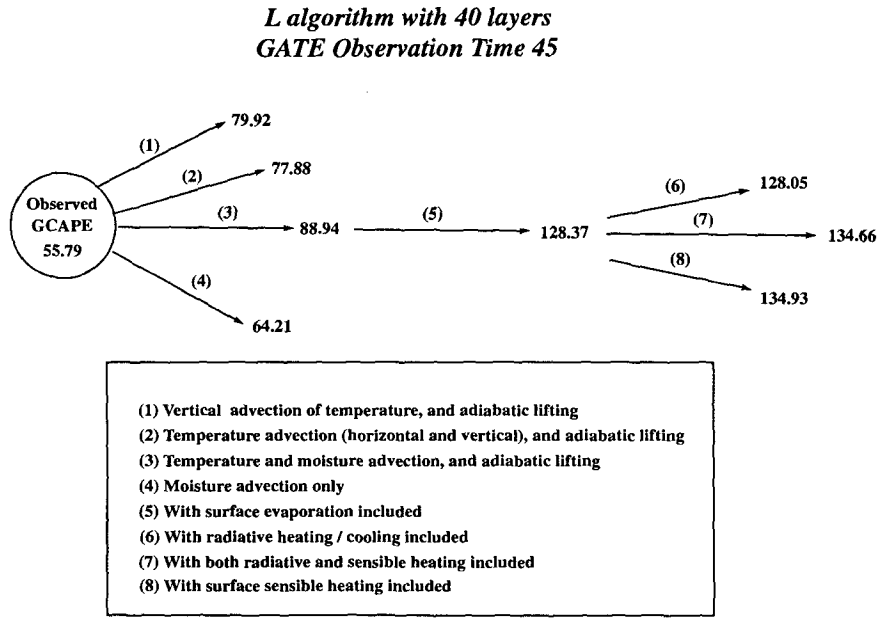

FIG. 6. For GATE Phase III observation time 45, the contributions of various processes to the GCAPE production rate. The circle represents the given state, and the numerical value inside gives the GCAPE of the given state, in J kg^{-1}. The arrows represent various nonconvective processes, acting over a three-hour period (see text). The numbers in parentheses next to the arrows refer to the legend in the box at the bottom of the diagram. The numbers at the ends of the arrows give the GCAPE obtained, in J kg^{-1}, after the action of the particular process over the specified three-hour period.

to nonconvective processes. Convection consumes GCAPE as fast as nonconvective processes can produce it. As a result, the atmosphere stays "close" to a neutral state (Arakawa and Schubert 1974), that is, the reference state. In Fig. 7, there appears to be some tendency for the strongest large-scale tendencies to be associated with negative observed time rates of change; this merits further investigation.

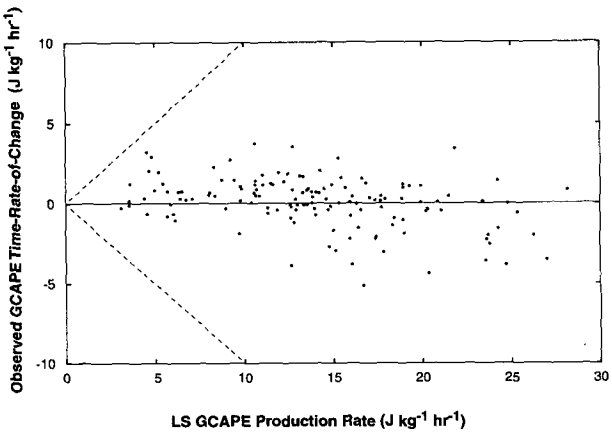

FIG. 7. A comparison of the rate of GCAPE production by large-scale processes (abscissa) and the observed rate of change of the GCAPE (ordinate). Each point represents one observation time.

As a sensitivity test, we changed Δt from 3 hours to 30 minutes; that is, we used the rates of change determined from the observations that are available once every 3 hours, but we applied these rates of change for

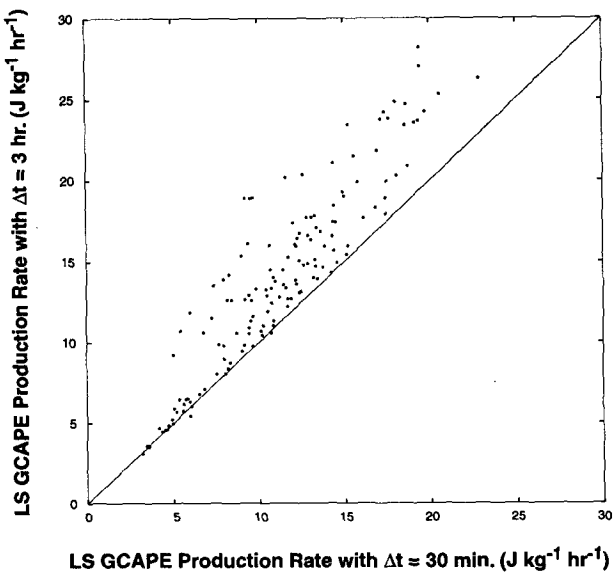

FIG. 8. A comparison of the magnitudes of the GCAPE production rates by large-scale processes with Δt = 30 min and Δt = 3 h.

only 30 minutes. Figure 8 shows that although the magnitudes of the GCAPE production rates by large-scale processes with $\Delta t = 30$ minutes are generally smaller than those with $\Delta t = 3$ h, the two estimates are nevertheless quite comparable. The positive correlations mentioned earlier, between the GCAPE production rate by the large-scale processes and the observed precipitation rate, are hardly affected. In short, our conclusions are not very sensitive to the value of Δt.

4. Summary and conclusions

Our analysis shows that both large-scale vertical motions and surface evaporation contribute significantly to the GCAPE production rate. The observed precipitation rate is negatively correlated (temporally) with the GCAPE, but is very positively correlated with the rate of GCAPE production by large-scale processes. The observed time rate of change of the GCAPE is much smaller than the rate of GCAPE production by nonconvective processes. This implies that the convection very efficiently consumes GCAPE, converting it into convective kinetic energy, in the sense that the rate of consumption of GCAPE by the convection is almost equal to the rate of production of GCAPE by nonconvective processes.

Our results encourage us to think that a cumulus parameterization can be formulated using the concept of GCAPE and its associated reference state. The equilibrium state to which the parameterization adjusts would be the reference state used in the definition of the GCAPE. An attractive aspect of this approach is that the equilibrium state is based neither on empiricism nor on simple cloud models, but rather on the basic physics of moist available potential energy.

The L algorithm used here uses a Lagrangian approach to find the GCAPE. It seems well suited to data analysis. As discussed in Part I, an Eulerian approach offers some advantages in modeling applications. This is a subject for further research.

Acknowledgments. Prof. W. H. Schubert and Dr. K.-M. Xu of CSU also offered comments on this work. Prof. R. Reed, of the University of Washington, allowed us to use the GATE data as analyzed by his group. Dr. E. E. Recker of the University of Washington helped us to obtain the evaporation and precipitation data. Professor M. Yanai, UCLA, supplied the GATE radiation data, as analyzed by Cox and Griffith (1979a,b).

Support has been provided by the National Aeronautics and Space Administration under Grant NAG5-1058 and the National Science Foundation under Grant ATM-8907414, both to Colorado State University. Computing resources were provided by the Scientific Computing Division of the National Center for Atmospheric Research, which is sponsored by the National Science Foundation.

APPENDIX

The Effects of Ice

a. Basic approach

For an air parcel consisting of one mass unit of dry air and $\bar{w}$ mass units of total water, of which w units are water vapor and $\bar{w} - w$ units are liquid water, the entropy s and enthalpy h can be expressed (Lorenz 1979) as

$$(1 + \bar{w})s = (c_p + \bar{w}c_{pw}) \ln T - R \ln(p - e) - \bar{w}R_w \ln(e) - (\bar{w} - w)\frac{L}{T} + \text{const}, \quad \text{(A.1)}$$

$$(1 + \bar{w})h = (c_p + \bar{w}c_{pw})T - (\bar{w} - w)L + \text{const}, \quad \text{(A.2)}$$

where T is air temperature, p is air pressure, e is water vapor pressure, R and R_w are the gas constants for dry air and water vapor, c_p and c_{pw} are the specific heat of dry air and water vapor at constant pressure, and L represents the latent heat from water vapor to liquid water. We want to consider the latent heat from water vapor to ice when the temperature is low enough.

From the Clausius–Clapeyron equation, $L(T)$ can be written as

$$L(T) = \frac{R_w T^2}{E(T)} \frac{dE(T)}{dT}, \quad \text{(A.3)}$$

where $E(T)$ is the saturation water vapor pressure at the temperature T. Substituting (A.3) into (A.1) and (A.2), and considering the saturated case, we obtain

$$(1 + \bar{w})s = (c_p + \bar{w}c_{pw}) \ln T - R \ln[p - E(T)] - \bar{w}R_w \ln[E(T)] - (\bar{w} - w)\left[\frac{R_w T}{E(T)} \frac{dE(T)}{dT}\right] + \text{const} \quad \text{(A.4)}$$

$$(1 + \bar{w})h = (c_p + \bar{w}c_{pw})T - (\bar{w} - w)\left[\frac{R_w T^2}{E(T)} \frac{dE(T)}{dT}\right] + \text{const}. \quad \text{(A.5)}$$

By using (A.4–5), the effects of ice can be included through the saturation vapor pressure, $E(T)$. We follow Ooyama's (1990) method to calculate $E(T)$.

Ooyama (1990) pointed out that there is a discontinuity, at 0°C, between the specific entropy of liquid water and that of ice. By defining a freezing zone of finite width, he eliminated this discontinuity, allowing ice effects to "ramp up" smoothly rather than "switch on" discontinuously. We apply his ideas to incorporate ice effects into the GCAPE calculation, as follows.

Ooyama considered the specific entropy of condensation for an air parcel, $C(T)$, as a weighted combi-

nation of the specific entropy of ice, $C_i(T)$, and the specific entropy of liquid water, $C_w(T)$:

$$C(T) = \Omega_w(T)C_w(T) + \Omega_i(T)C_i(T). \quad \text{(A.6)}$$

Here $\Omega_w(T)$ and $\Omega_i(T)$ are smooth functions:

$$\Omega_w(T) = \frac{1}{2}\left[1 + \tanh\left(\frac{T - T_f}{\Delta T_f}\right)\right],$$

$$\Omega_i(T) = 1 - \Omega_w(T);$$

ΔT_f is the width of the "freezing zone"; and T_f is the central temperature of the freezing zone. The expressions for $C(T)$, $C_i(T)$, and $C_w(T)$ are

$$C_w(T) = C_{pw}\ln\left(\frac{T}{T_0}\right) - R_w\frac{d}{dT}\left[T\ln\left(\frac{E_w(T)}{E_{w0}}\right)\right] + \text{const}, \quad \text{(A.7)}$$

$$C_i(T) = C_{pw}\ln\left(\frac{T}{T_0}\right) - R_w\frac{d}{dT}\left[T\ln\left(\frac{E_i(T)}{E_{i0}}\right)\right] + \text{const}, \quad \text{(A.8)}$$

$$C(T) = C_{pw}\ln\left(\frac{T}{T_0}\right) - R_w\frac{d}{dT}\left[T\ln\left(\frac{E(T)}{E_{w0}}\right)\right] + \text{const}, \quad \text{(A.9)}$$

where $E_w(T)$ is the saturation water vapor pressure over a liquid water surface at temperature T, and $E_i(T)$ is the saturation water vapor pressure over an ice surface at temperature T. Also, $E_{w0} = 6.108$ mb is the saturation water vapor pressure over a liquid water surface at the temperature $T_0 = 273.16$ K, and $E_{i0} = 6.107$ mb is the saturation water vapor pressure over an ice surface at T_0.

Substituting (A.7), (A.8), and (A.9) into (A.6), we find that

$$\frac{d}{dT}\left[T\ln\left(\frac{E(T)}{E_{w0}}\right)\right] = \Omega_w(T)\left[T\ln\left(\frac{E_w(T)}{E_{w0}}\right)\right] + \Omega_i(T)\left[T\ln\left(\frac{E_i(T)}{E_{i0}}\right)\right]. \quad \text{(A.10)}$$

As a boundary condition, we use $E(T_s) \to E_w(T_s)$ for $T_s \gg T_f$, where $T_s = 350$ K. Integrating (A.10), we obtain

$$\left[T\ln\left(\frac{E(T)}{E_{w0}}\right)\right]\Bigg|_{T_s}^{T} = \left[\Omega_w(T)T\ln\left(\frac{E_w(T)}{E_{w0}}\right) + \Omega_i(T)T\ln\left(\frac{E_i(T)}{E_{i0}}\right)\right]\Bigg|_{T_s}^{T}$$

$$- \int_{T_s}^{T} T\ln\left[\frac{E_w(T)}{E_{w0}}\right] d\Omega_w(T) - \int_{T_s}^{T} T\ln\left[\frac{E_i(T)}{E_{i0}}\right] d\Omega_i(T). \quad \text{(A.11)}$$

We have adopted the formulas for $E_w(T)$ and $E_i(T)$ given in the Smithsonian meteorological tables. With (A.11), these can be used to evaluate $E(T)$.

In this paper, we have used $T_f = 270.16$ K, and $\Delta T_f = 3$ K; this corresponds to a "freezing zone" from −6°C to 0°C. Naturally, these choices have some influence on the results that we obtain. As an example, Fig. A1 shows the GCAPE and the large-scale tendency of the GCAPE obtained with two different choices of ΔT_f. The differences are modest.

b. *Sensitivity of the GCAPE to ice effects*

The increase of the GCAPE due to ice effects, as obtained with the L algorithm, is surprisingly large: ice effects cause the GCAPE to increase from 12.6 J kg^{-1} to 56 J kg^{-1}, with 40 layers.

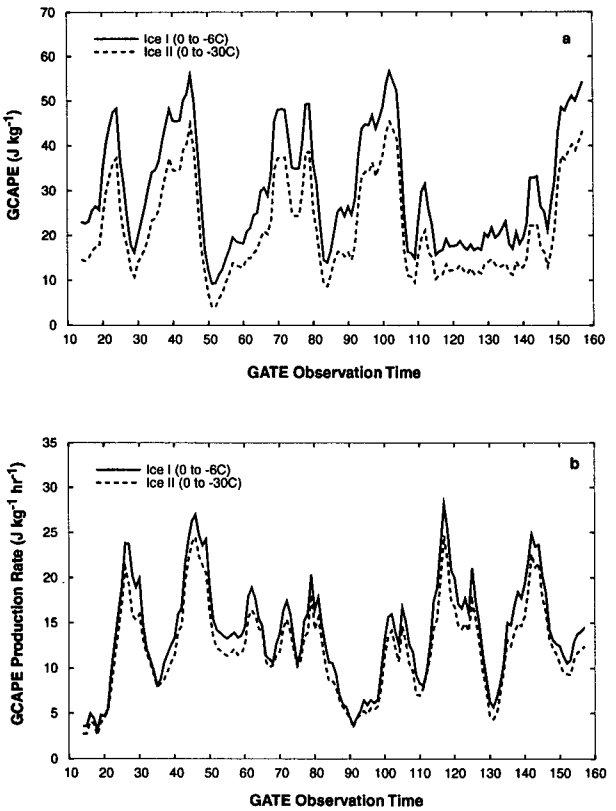

FIG. A1. Time history of the GCAPE (panel a) and the GCAPE production rate by large-scale processes (panel b), as obtained with "freezing zones" that extend from 0°C to −6°C (solid lines) and from 0°C to −30°C (dashed lines).

To investigate the reason for the peculiar sensitivity of the L algorithm, we use GATE observation time 45 as an example. We divide the sounding into 20 layers, numbered from the top down. By using the no-ice version of the L algorithm, we find that the reference state can be reached by moving parcel 20 of the given state to the position of parcel 2 of the given state, and shifting parcels 2 through 19 down by one level. In passing from the given state to the reference state, the enthalpy of layer 1 remains unchanged, the enthalpy of layer 2 is reduced, and the enthalpies of layers 3 to 20 are increased. The total enthalpy increase of layers 3 to 20 is less than the enthalpy decrease of layer 2; that is, the system's total enthalpy decreases, by 10 J kg^{-1}.

Referring to (A.2), we see that the enthalpy per unit mass thus consists of a temperature component [the first term on the rhs of (A.2)] and a liquid/ice component (the second term). For the lifted parcel, the change due to condensate is negative, while the change due to warming is actually positive. For the subsiding parcels, the change due to warming is positive, while the change in the liquid/ice component is zero. For the entire column, warming increases the enthalpy by 2270.1 J kg^{-1}, while condensation decreases the enthalpy by 2280.1 J kg^{-1}. The net decrease in the enthalpy, 10 J kg^{-1}, is the small difference between these large numbers.

Now suppose that ice effects are included. Not surprisingly, it turns out that the parcels are rearranged in the same way as before. The GCAPE is 57.2 J kg^{-1} this time, however! Obviously, ice formation influences only the enthalpy of the upward-moving parcel; it has no effect on the enthalpy of the subsiding, ice-free parcels. The temperature of the lifted parcel increases, but its condensate mixing ratio also increases; according to (A.2), the warming increases the enthalpy, but the additional condensate decreases the enthalpy. The additional warming due to ice is 2.25 K. On the other hand, the additional condensate formed amounts to 1.3×10^{-2} g kg^{-1}. For the whole column, warming increases the enthalpy by 2384.6 J kg^{-1}, while the formation of liquid and ice decreases it by 2441.8 J kg^{-1}. The net effect of ice, therefore, is to decrease the enthalpy by 47.2 J kg^{-1}, implying an increase of the GCAPE by the same amount. This is an enormous increase from the 10 J kg^{-1} obtained without ice, but is not much compared to the individual "warming" and "condensate" terms that nearly cancel.

REFERENCES

Arakawa, A., and W. H. Schubert, 1974: The interaction of a cumulus cloud ensemble with large-scale environment, Part I. *J. Atmos. Sci.*, **31**, 674–701.

Cox, S. K., and K. T. Griffith, 1979a: Estimates of radiative divergence during Phase III of the GARP Atlantic Tropical Experiment. Part I: Methodology. *J. Atmos. Sci.*, **36**, 576–585.

——, and ——, 1979b: Estimates of radiative divergence during Phase III of the GARP Atlantic Tropical Experiment. Part II: Analysis of Phase III Results. *J. Atmos. Sci.*, **36**, 586–601.

Lord, S. J., 1982: Interaction of a cumulus cloud ensemble with the large-scale environment. Part III: Semi-prognostic test of the Arakawa–Schubert cumulus parameterization. *J. Atmos. Sci.*, **39**, 88–103.

Lorenz, E. N., 1955: Available potential energy and the maintenance of the general circulation. *Tellus*, **7**, 157–167.

——, 1978: Available energy and the maintenance of a moist circulation. *Tellus*, **30**, 15–31.

——, 1979: Numerical evaluation of moist available energy. *Tellus*, **31**, 230–235.

Ooyama, K. V., 1990: A thermodynamic foundation for modeling the moist atmosphere. *J. Atmos. Sci.*, **47**, 2580–2593.

Randall, D. A., and J. Wang, 1992: The moist available energy of a conditionally unstable atmosphere. *J. Atmos. Sci.*, **49**, 240–255.

Thompson, R. M., Jr., 1977: Preliminary heat and moisture budgets over the B-scale ship array during Phase III of GATE. M.S. thesis, University of Washington, 103 pp.

——, S. W. Payne, E. E. Recker, and R. J. Reed, 1979: Structure and properties of synoptic scale wave disturbances in the intertropical convergence zone of the eastern Atlantic. *J. Atmos. Sci.*, **36**, 53–72.

Xu, K.-M., and A. Arakawa, 1992: Semiprognostic tests of the Arakawa–Schubert cumulus parameterization using simulated data. *J. Atmos. Sci.*, **49**, 2421–2436.